

International Conference on Space Optics—ICSO 2022

Dubrovnik, Croatia

3–7 October 2022

Edited by Kyriaki Minoglou, Nikos Karafolas, and Bruno Cugny,



Impact of Straylight in Michelson Fourier transform spectrometers



Impact of Straylight in Michelson Fourier transform spectrometers

Pierre Dussarrat^{*a}, Guillaume Deschamps^a, Sahar Dehnavi^b, Bertrand Theodore^a, Dorothee Coppens^a

^aEuropean Organisation for the Exploitation of Meteorological Satellites (EUMETSAT)

^bHE Space Operations GmbH

*pierre.dussarrat@eumetsat.int

ABSTRACT

Atmospheric remote sensing using long wave infrared (LWIR) **Fourier transform spectrometers** (FTS) has become in the last 20 years a key component of the Earth monitoring system. Their large coverage and deci-kelvin accuracy have demonstrated their usefulness in weather prediction, atmospheric composition measurements as well as climate monitoring. It is thus critical to investigate the possible sources of errors associated to this technique. One of them is the impact of light spurious reflections and scattering inside the instrument, the so-called **straylight**. The theoretical description of the effect is presented in the context of **Michelson interferometers**, then, several correction methodologies and associated processing have been designed and their performances are assessed.

Keywords: Fourier transform spectrometer, straylight, Michelson interferometer.

1. INTRODUCTION

Fourier transform spectrometry is a powerful mean to sound the atmosphere by resolving the spectral lines of the infrared radiation emitted by the Earth and the atmosphere. The light enters the instrument, which is mainly composed of a telescope and a two-arms interferometer. The interference pattern is recorded on the instrument detector as a function of the difference between the length of the two arms, called the optical path distance (OPD). The spectral radiance is recovered by Fourier transform of the interferogram. Finally, the spectrum exhibits absorption and emission lines representative of the Earth atmosphere composition and thermodynamic state.

One possible source of error associated to such a measure is straylight: indeed, as the optics coating and cleanliness of the optics are never perfect, it is likely that a pixel receives light from outside of the nominal optical path. The light can be, for example, reflected multiple times inside the instrument or scattered on rough surfaces.

In the current and future low-orbit missions such as IASI (METOP), IASI-NG (METOP-SG), CrIS (Suomi NPP) or HIRAS (FY-3), the pixel's field of views (FOV) are physically separated by a cold plate placed at the instrument focal plane that efficiently blocks most of the straylight. However, in the next generation of geostationary spectro-imagers, such as GIIRS (FY-4) and IRS (MTG-S), the Earth disk is scanned without gaps using contiguous pixels placed directly at the focal plane. Therefore, we expect in that case a possible significant impact of straylight. That is why the authors have initiated this study in order to anticipate the corrections possibly needed in processing the data of these future instruments.

Straylight contamination and correction algorithms have been extensively studied for a wide range of instruments. It is well known that, by means of image deconvolution by the instrument spatial response [1], it is possible to cancel or at least mitigate the effect of straylight. The case of a Michelson-based Fourier transform spectro-imager goes however beyond the scope of the previous studies: in this paper, we will indeed show that a "standard" deconvolution efficiency is actually limited as the interferences are FOV-dependent. We will establish that the measured spectra are composed of a linear sum of spectral radiances weighted by the spatial response but also shifted by a FOV-dependent spectral scaling.

Section 2 proposes a theoretical description of the impact of straylight on spectra measured by a spectro-imager and presents simulations representative of measurements performed from geostationary instrument. In section 3, we several

correction strategies are considered and their performances are assessed. Section 4 discusses the limitations of the model and the remaining open-questions.

2. STRAYLIGHT IMPACT

2.1 Instrument description

A Fourier Transform Spectrometer (FTS) typically includes of a front telescope (FT) that collects the radiation exiting the Earth, a Michelson interferometer that splits the light into two arms and recombine it afterward, a back telescope (BT) and a detection assembly (DA) including a detector; in this paper we consider a detector array i.e. a matrix of contiguous pixel. Moreover, a field stop is placed inside the front telescope to limit the FOV.

In this paper, we discuss for simplicity only the straylight occurring after the front telescope. The following diagram describes the light propagation through the instrument; the dotted arrows represent the straylight:



We make the following definitions and hypotheses about the instrument:

- The FOV angle $\theta_{i,j}$ are defined at interferometer level and are indexed by the related pixel detector matrix row and column indexes (i,j) . We assume that the pixels are covering the whole instrument FOV without gaps.
- To describe the straylight properties, we use the Intensity Point Spread Function (IPSF), which describes the angular distribution of light reaching each pixel. Figure 1 shows examples of such IPSFs including a straylight background.
The IPSFs for every pixel of the detector (I,J) are defined over the full FOV i.e. as function of the instrument pixels (i,j) and as function of the wavenumber ν : $IPSF_{i,j}(i,j,\nu)$.
- We define the signal entering the instrument $Sp(i,j,\nu)$ with its power spectrum distribution as function of the wavenumber ν and indexed by the instrument pixels as well (Figures 2, 3 and 4).

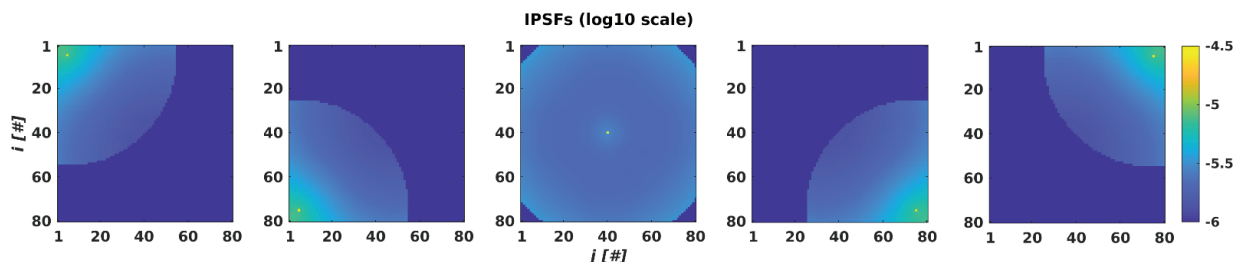


Figure 1. Intensity Point Spread Function (IPSF) describing the angular distribution of light reaching five pixels of the detector (corners and centre) in log10 scale. The IPSF are presented on the instrument full FOV and at pixel sampling (80x80). The IPSFs exhibit a peak representative of the nominal light path of amplitude 0.99 and a circular mid-range background representative of the straylight summing to 0.01.

2.2 Straylight equation

Each pixel records an interferogram as a function of the interferometer arm's length difference x . Following Michelson's equations [3], the OPD is FOV dependent and should be multiplied by $\cos(\theta_{i,j})$. Accounting for all wavenumber components of the input spectrum $Sp(i, j, \nu)$ and finally applying the spatial convolution with the IPSF, the raw interferograms $I_0(I, J, x)$ write (Eq. 1):

$$I_0(I, J, x) \propto \sum_{i,j} \int d\nu \text{IPSF}_{i,j}(\nu) \times Sp(i, j, \nu) \times \cos(2\pi\nu x \times \cos(\theta_{i,j}))$$

We assume that the interferograms are re-sampled on board on a common OPD grid using a laser-based metrology system similar to the one used in IASI or IRS. This resampling counters partially the scaling effect for all pixels of interest (I,J) dividing the OPD by $\cos(\theta_{i,j})$. The resampled interferograms then write (Eq. 2):

$$I_m(I, J, x) \propto \sum_{i,j} \int d\nu \text{IPSF}_{i,j}(\nu) \times Sp(i, j, \nu) \times \cos\left(2\pi\nu x \times \frac{\cos(\theta_{i,j})}{\cos(\theta_{i,j})}\right)$$

Finally, assuming a small FOV ($\theta_{i,j} \ll 1$) and assuming that the IPFSs slowly depend on wavenumbers, we compute the measured spectrum $Sp_m(I, J, \nu)$ by inverse Fourier transform and applying a radiometric calibration (Eq. 3):

$$Sp_m(I, J, \nu) = \sum_{i,j} \text{IPSF}_{i,j}(\nu) Sp\left(i, j, \nu \times \frac{\cos(\theta_{i,j})}{\cos(\theta_{i,j})}\right)$$

The measured spectrum thus results from the combination of two effects:

- First, the usual convolution of the input scene with the IPSF as expected for any imager;
- Second, a scaling of the spectra as a function of the FOV.

The latter is specific to Michelson-based FTS and therefore makes the impact of straylight in such instruments differing from the usual case of the imagers.

2.3 Simulation

In order to assess the validity of the theoretical description, we have simulated the effect of straylight in the long-wave infrared (LWIR) band of a Fourier transform spectro-imager. Parameters of the simulation are chosen such that the simulated instrument resembles MTG-S IRS [2]. Nonetheless, the IPSFs used for the simulation are made-up specifically for this study and are not expected to be representative of the actual instrument.

We consider a square field-stop that limits the FOV to ± 2 degrees at interferometer level. The FOV is fully covered with 80x80 pixels; note that the number of pixels is down-scaled by a factor four with respect to IRS in order to speed-up the computations.

The IPSFs consist in a peak at the pixel position with an amplitude of 0.99 corresponding to the nominal light path. In order to simulate the straylight, a circular background with a radius of 50 pixels is introduced around the central peak such that the total energy out of the nominal path is 0.01. As the purpose of the study is to analyze the effect of mid-range straylight, we neglect the effect of wave-front error and diffraction. These simulated IPSFs could be representative of scattering or un-focused reflections inside the instrument. They are represented on figure 1 for five pixels (corners and center). For simplicity, the simulated IPSFs have no wavenumber dependency.

Three distinctive scenes representative of what would be measured from the geostationary orbit at zero degree longitude have been used in this study. The spectra are computed using a radiative transfer model (RTTOV [6]) set-up to generate IASI-like spectra between 650 and 1250 cm^{-1} at 0.25 cm^{-1} sampling from which raw interferograms are computed

following in Eq. 1 after removal of the IASI numerical apodisation. On-board resampling is simulated by spline interpolation on a common OPD grid ranging between $\pm 8.2\text{mm}$. Finally, we apply the MTG-S IRS numerical apodisation and perform the inverse Fourier transform to retrieve the spectra. The generated spectra are sampled at 0.61cm^{-1} .

A run using point-like IPSFs is used as the reference to evaluate the radiometric error induced by the presence of the defined mid-range straylight. The radiometric errors are converted from radiance to equivalent temperature error dividing by the derivative of the Planck function at 280K.

In the following plots are shown, for each case:

- the average band radiance for the 80x80 pixels (top-left);
- the average and standard deviation of the errors induced by straylight (top-right);
- a selection of 10 spectra from the hottest to coldest average radiance (bottom-left) and their related errors (bottom-right).

- **Uniform scene:**

The first studied scene is almost *uniform*; it is representative of a clear sky over the north Atlantic sea. Results are shown on Fig. 2. In this case, the straylight produces pixel dependent error oscillations and spikes. The errors reach approximately 200mK around 750cm^{-1} wavenumber. As discussed in section 3.2, this error pattern is interpreted as a distortion of the instrument spectral response functions.

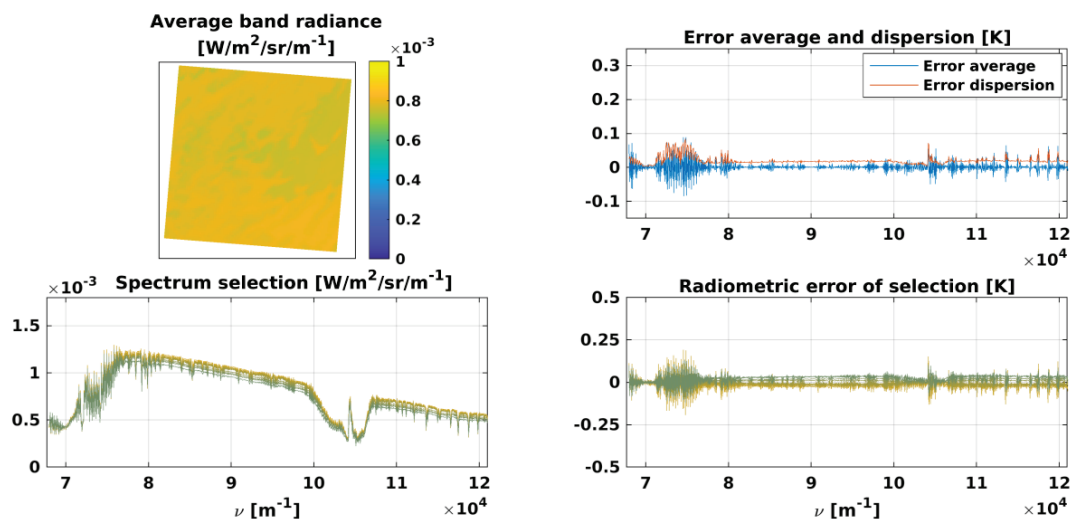


Figure 2. Straylight impact on a *uniform* scene (North Atlantic sea without clouds). The radiometric errors are presented as equivalent temperature error for a black body at 280K.

- **Contrasted scene:**

The second scene is contrasted: it is representative of a mix of clear and cloudy pixels over the French south coast. Fig. 3 shows that even if there are still error spikes visible in the error average, the errors are now dominated by a strong

dispersion. The errors reach approximately 300mK for the coldest spectrum. Due to the mid-range IPSF extension the whole scene is mixed on the detector, therefore the hottest spectra are measured too cold and the coldest spectra too hot.

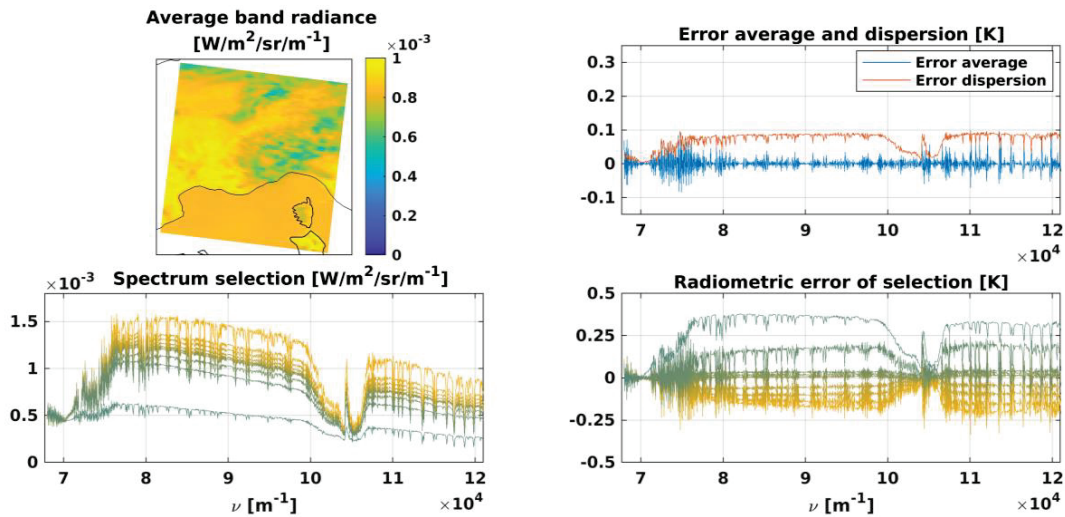


Figure 3. Straylight impact on a *contrasted* scene (French south coast including clouds). The radiometric errors are presented as equivalent temperature error for a black body at 280K.

- Limb:

The last scene is taken on the *limb* over North America. This represents the highest degree of contrast one can expect from a MTG-S IRS-like instrument and Fig. 4 shows that, as for the case of a contrasted scene, the errors are dominated by scene-mixing. Some Earth signal is projected in space and therefore the Earth side is measured too cold.

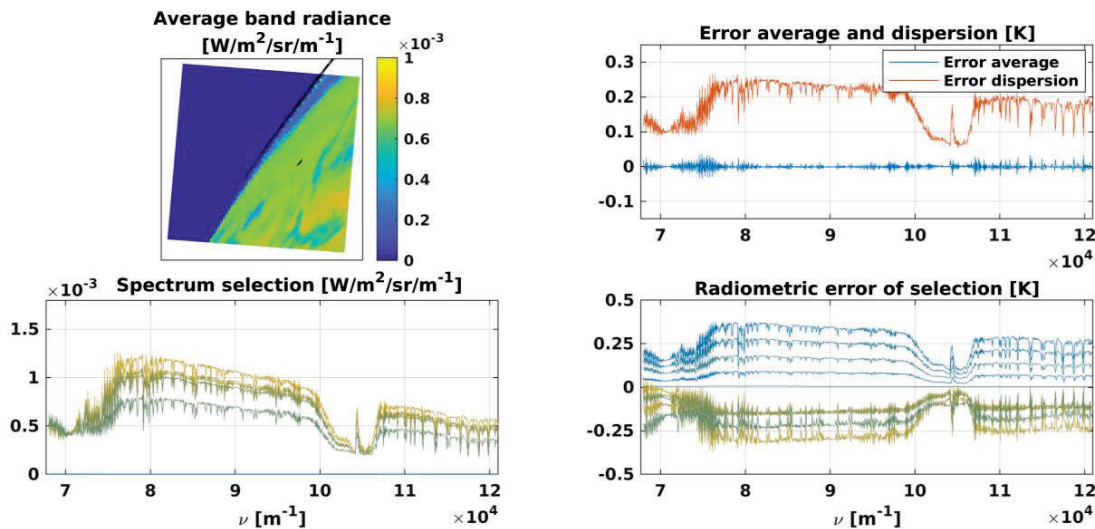


Figure 4. Straylight impact on a *limb* scene (Limb over North America). The radiometric errors are presented as equivalent temperature error for a black body at 280K.

From the analysis of the simulation, we retrieve what the theoretical derivation has shown: the straylight produces two effects:

- error oscillations and spikes particularly visible for the uniform scene;
- a loss of contrast.

The first effect is representative of spectral response function distortions and the second one of a scene mixing induced by the IPSF mid-range background.

It is worth noting that one can detect the presence of straylight from the measurements of any instrument by two means:

- Remaining signal appearing outside of the earth rim,
- Analysis of the instrument radiometric calibration as function of the spectra average temperature. One should assess if the hottest spectra are measured too cold and the coldest spectra too hot as in figures 3 and 4. Such a radiometric analysis can be conducted using colocations with other instruments or comparison to radiative transfer models. The authors have for example performed such an analysis for the FY-4A GIRS instrument comparing to IASI [4].

The simulations show that a background of only 1% can cause radiometric errors up to 300mK, larger than the typical radiometric calibration target of 100mK. Therefore, mitigation strategies; exposed in the next section, have been devised.

3. STRAYLIGHT CORRECTION

In the following sections, we aim at designing a post-processing using the measured spectra $Sp_m(I, J, \nu)$ that would limit the effect of straylight.

3.1 Full correction

To cancel the effect of straylight, we can first try to inverse equation 3. Considering that the IPSFs amplitudes are small out of their central part and a small FOV ($\theta_{i,j} \ll 1$), one can derive the following *full correction* equation (Eq. 4):

$$Sp_{full}(I, J, \nu) = \frac{1}{IPSF_{I,J}(I, J, \nu)} \times \left\{ Sp_m(I, J, \nu) - \sum_{i,j \neq I,J} IPSF_{I,J}(i, j, \nu) Sp_m \left(i, j, \nu \times \frac{\cos(\theta_{i,j})}{\cos(\theta_{I,J})} \right) \right\}$$

The corrected spectra Sp_{full} are in that case computed by a first order deconvolution coupled with the appropriate spectral scaling.

This approach however faces a major computational issue: in order to correct each pixel (I, J) , applying spectral shifts to all other measured spectra (i, j) is required. This means a number of shifts that scales with the number of pixels square. Therefore, the computation time becomes unrealistic if the number of pixels reaches a few thousands (e.g. in the case of

a IRS). Note that this complexity is closely related to the fact that we assume a resampling on board before any straylight correction.

In conclusion, due to its unacceptable technical burden, the *full correction* method has been discarded and not assessed in this paper. In the following, we will focus on two simplified methodologies.

3.2 Uniformisation

In this section, we first assume that the input scene is spatially uniform $Sp(v)$ and derive an adequate straylight correction equation.

We compute an alternate form of the resampled interferogram $I_u(I, J, x) = FT[Sp_m(I, J, v)]$, assuming a small FOV ($\theta_{i,j} \ll 1$), we show that the straylight acts as an interferogram self-apodisation (Eq. 5):

$$\begin{aligned} I_u(I, J, x) &= FT[Sp_m(I, J, v)] = \int dv \sum_{i,j} IPSF_{i,j}(i, j, v) Sp\left(v \times \frac{\cos(\theta_{i,j})}{\cos(\theta_{i,j})}\right) \exp(-2i\pi vx) \\ &= \int dv Sp(v) \exp(-2i\pi vx) \times SAF_{stray}(I, J, v, x) \end{aligned}$$

With the following self-apodisation functions (SAF) (Eq. 6):

$$SAF_{stray}(I, J, v, x) = \sum_{i,j} IPSF_{i,j}(i, j, v) \exp\left(2i\pi vx \times \left[1 - \frac{\cos(\theta_{i,j})}{\cos(\theta_{i,j})}\right]\right)$$

This can be interpreted as a distortion of the instrument spectral response functions as a function of the pixel locations and wavenumber. It is closely related to the FOV dependent spectral scaling present in equation 3: this distortion is a characteristic of the Michelson configuration.

Figure 5 presents the SAF real and imaginary parts for the central and corner pixels at four wavenumbers. It clearly shows that the self-apodisation slowly depends on the wavenumber and therefore validate the use of a limited set in the correction.

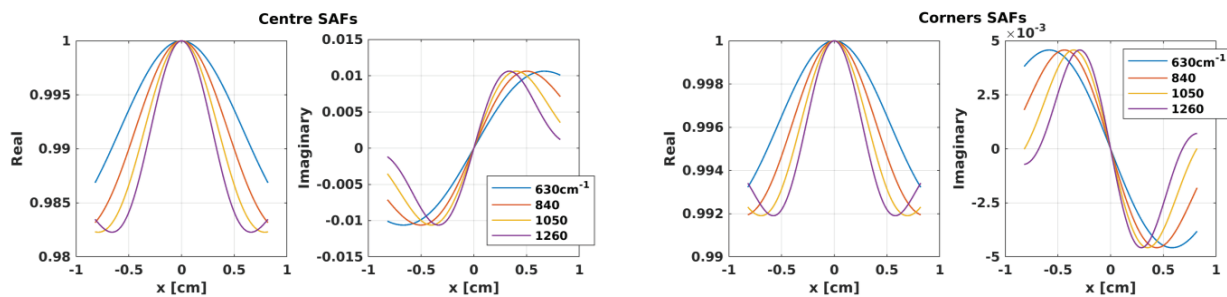


Figure 5. Self-apodisation functions for the central pixel and corner pixels, the real and imaginary parts represented for four wavenumbers of the band.

The self-apodisations are cancelled at interferogram level by dividing the Fourier transform of the measured spectra $FT[Sp_m(I, J)]$ by the SAFs at wavenumbers ν_k , then we apply again the inverse Fourier transform and retrieve a set of corrected spectra Sp_{u, ν_k} (Eq. 7):

$$Sp_{u, \nu_k}(I, J, \nu) = FT^{-1} \left[\frac{FT[Sp_m(I, J, \nu)]}{SAF_{stray}(I, J, \nu_k, x)} \right]$$

Finally, we recover the "uniformised" spectrum Sp_u at all wavenumbers by linear interpolation of the Sp_{u, ν_k} as follow (Eq. 8):

$$Sp_u(I, J, \nu \in [\nu_k, \nu_{k+1}]) = \frac{\nu - \nu_{k+1}}{\nu_k - \nu_{k+1}} \times Sp_{u, \nu_k}(I, J, \nu) + \frac{\nu_k - \nu}{\nu_k - \nu_{k+1}} \times Sp_{u, \nu_{k+1}}(I, J, \nu)$$

Note that an analog uniformisation processing is performed routinely in most hyperspectral instruments such as IASI, CrIS and is expected to be implemented for IRS to cancel other sources of self-apodisation. Therefore, the straylight uniformisation would not require extra processing time.

We apply the straylight uniformisation using one hundred SAFs evenly spaced in the spectral band to all three scenes introduced in 2.3. Results are shown on Fig. 6. As expected, it effectively reduces the errors of the uniform scene. For the contrasted and limb scenes, however, the impact on the error dispersion is limited even if the average error is effectively decreased.

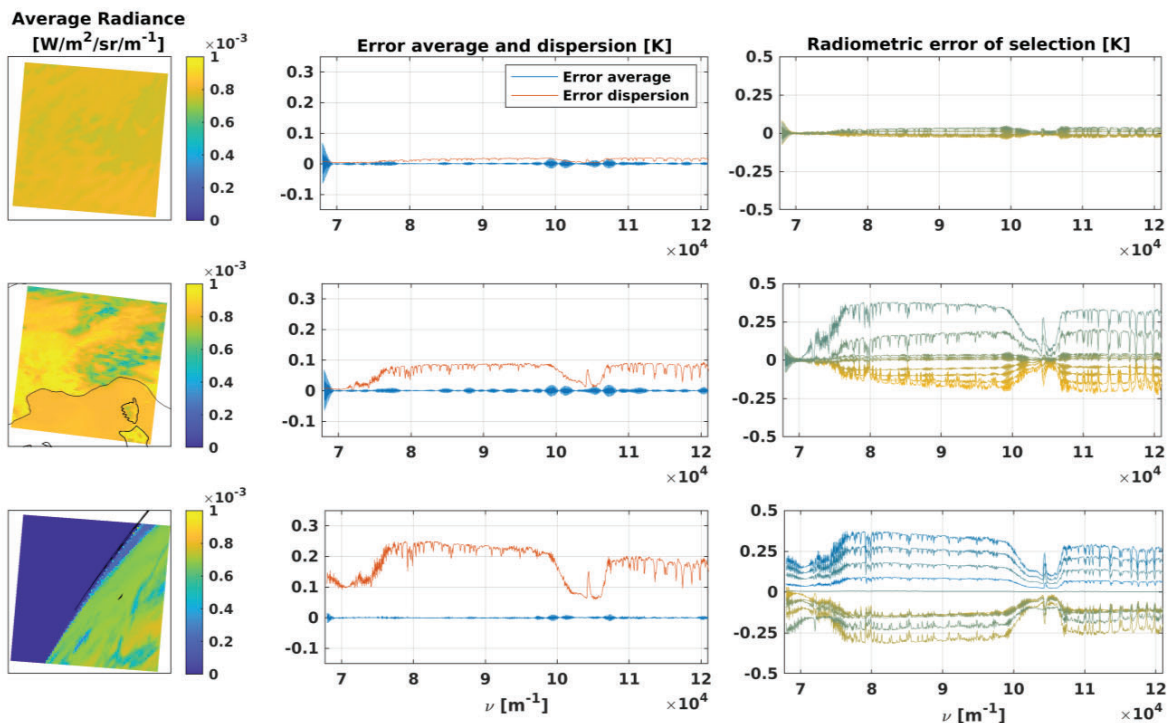


Figure 6. Straylight mitigation by uniformisation for three scenes. The radiometric errors are presented as equivalent temperature error for a black body at 280K.

3.3 Deconvolution

In order to tackle the high dispersion of the error induced by scene mixing, we propose to neglect the spectral scaling and apply a deconvolution as for an imager. Considering that the IPSFs amplitudes are small out of their central part, the *deconvolution* writes (Eq. 9):

$$Sp_{deconv}(I, J, \nu) = \frac{1}{IPSF_{I,J}(I, J, \nu)} \times \left\{ Sp_m(I, J, \nu) - \sum_{i,j \neq I,J} IPSF_{I,J}(i, j, \nu) Sp_m(i, j, \nu) \right\}$$

Note that in general, the deconvolution should be performed at all wavenumbers. In practice, the IPSF depends only slowly on the wavenumber, which allows performing the deconvolution for a limited set of wavenumbers and recombine the solutions by linear interpolation.

We apply the deconvolution to all three scenes introduced in 2.3. Figure 7 shows that, as expected, it reduces the scene-mixing effect and effectively decreases the error dispersion for the contrasted and limb scenes. Nonetheless, the deconvolution has no impact on the average error and some oscillations and spikes remain in the errors.

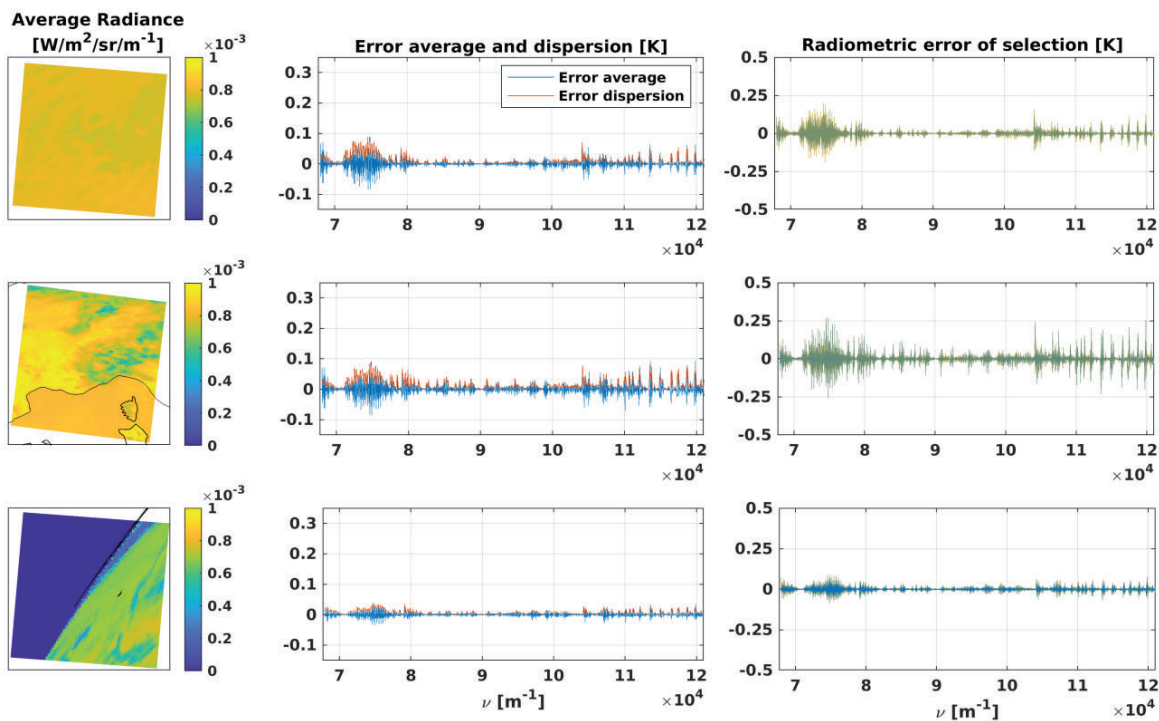


Figure 7. Straylight mitigation by deconvolution for three scenes. The radiometric errors are presented as equivalent temperature error for a black body at 280K.

3.4 Fast correction

Finally, taking advantage of both technics, we propose to combine the *uniformisation* and *deconvolution*; this is referred to as the *fast correction*. We first apply the uniformisation and then the deconvolution to all three scenes introduced in 2.3.

Comparing the final performances of the *fast correction* to the expected straylight impact in section 2.3, Fig. 8 shows that it is possible to achieve a shrink of the errors by approximately a factor 10. The error average is efficiently reduced by the uniformisation and the dispersion by the deconvolution.

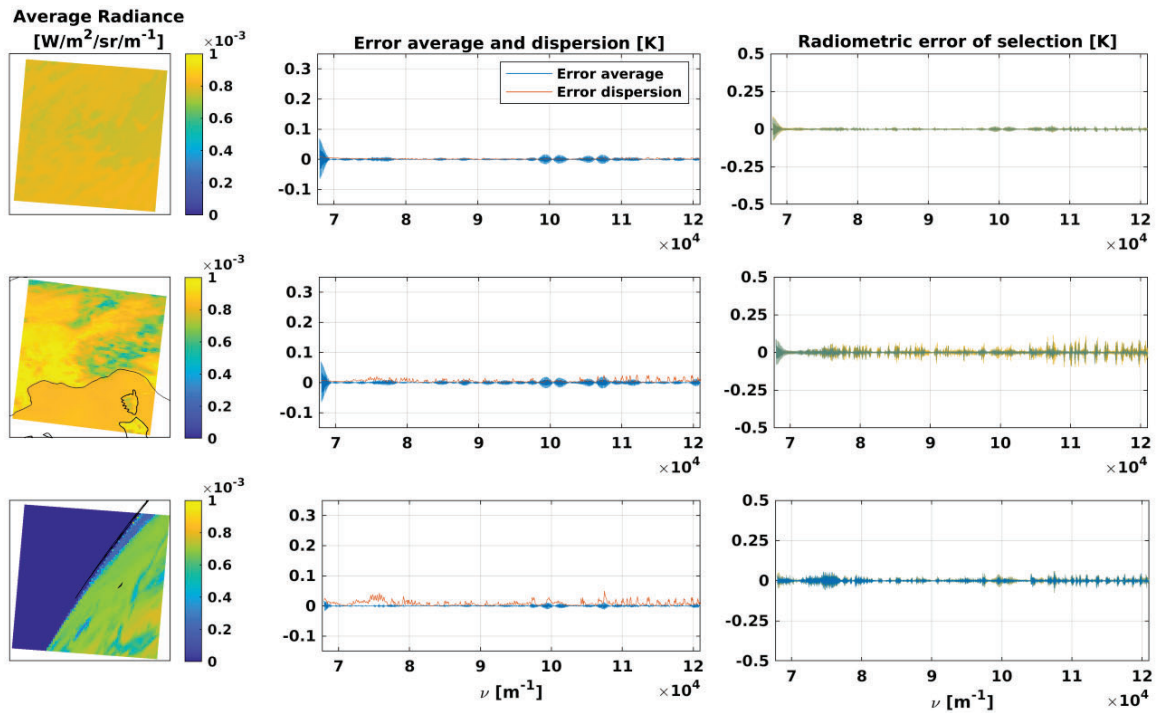


Figure 8. Straylight mitigation by fast correction for three scenes. The radiometric errors are presented as equivalent temperature error for a black body at 280K.

The maximal errors are finally constrained below 50mK for almost all spectra, which validates the approach. The remaining spikes for the contrasted and limb scenes (middle and bottom-right panels of figure 8) come from the approximation of uniform scene in the uniformisation processing which is not met for these cases.

4. DISCUSSION

We finally discuss several points of limitations of this study and open questions for the future of straylight correction in Fourier transform spectrometers:

- The simulations were performed with an IPSF independent of the wavenumber. In practice, the coating and scattering properties could strongly depend on the wavenumber. The uniformisation is already wavenumber-dependent but then the deconvolution part should be performed for a few wavenumbers and the solution reconstructed by linear interpolation.
- The derivations neglect any zero path distances (ZPD) of the interferometer as function of the FOV; this can however be added in the SAFs computation in equation 6.
- The assumptions that the detector covers the full FOV is strong. In practice, parts of the FOV can be lost between the pixel matrix edge and the field stop. This will directly affect the deconvolution efficiency.
- Field compensation optics as the double prism in the Mertz interferometer used for IASI-NG [5] cancels the OPD dependency with the FOV. In that case, only a deconvolution would be required.

5. CONCLUSION

In conclusion, we have theoretically established that the presence of straylight inside a spectrometer using a Michelson interferometer is producing detrimental radiometric error. The measured spectra appear convoluted with the instrument IPSF but also include wavenumber scaling.

In this paper, different scenes, typical from what could be recorded from the geostationary orbit, have been used: a uniform, a contrasted and a limb view. The simulation shows that a straylight background accounting for only 1% of the total energy is causing scene dependent radiometric error up to 300mK.

We have first considered the *full correction*; however it is not technically feasible, as it requires a number of spectra shifts scaling as the number of pixel square. We have thus proposed two other methods, one relying on an *uniformisation* and the other on a *deconvolution*. The uniformisation mitigates the spectral response function distortions caused by straylight while the deconvolution cancels the scene mixing effect. Combining both methods results in the *fast correction*, with which we are able to achieve a significant mitigation of the straylight impact on the radiometric calibration: the error is reduced by a factor 10 and remains below 50mK for most spectra.

REFERENCES

- [1] Starck, J. L., Pantin, E., & Murtagh, F. (2002). Deconvolution in astronomy: A review. Publications of the Astronomical Society of the Pacific, 114(800), 1051.
- [2] <https://www.eumetsat.int/mtg-infrared-sounder>
- [3] Hariharan, P. (2010). Basics of interferometry. Elsevier.
- [4] Dussarrat, P., & Burrows, C. (2022). Technical Memo.
- [5] F. Bermudo, S. Rousseau, E. Pequignot and F. Bernard, "IASI-NG program: A new generation of Infrared Atmospheric Sounding Interferometer," 2014 IEEE Geoscience and Remote Sensing Symposium.
- [6] Saunders, R., Hocking, J., Turner, E., Rayer, P., Rundle, D., Brunel, P., Vidot, J., Roquet, P., Matricardi, M., Geer, A., Bormann, N., and Lupu, C., 2018: An update on the RTTOV fast radiative transfer model (currently at version 12), Geosci. Model Dev., 11, 2717-2737, <https://doi.org/10.5194/gmd-11-2717-2018>.